Proximity Relationships between Residue 6 of Troponin I and Residues in Troponin C: Further Evidence for Extended Conformation of Troponin C in the Troponin Complex†

Yin Luo,‡ John Leszyk,§ Bing Li,‡ John Gergely,‡,||,⊥ and Terence Tao*,‡,#,◇

Muscle Research Group, Boston Biomedical Research Institute, Watertown, Massachusetts 02472, Neurology Service, Massachusetts General Hospital, Boston, Massachusetts 02114, Departments of Biological Chemistry and Molecular Pharmacology and of Neurology, Harvard Medical School, Boston, Massachusetts 02115, Department of Biochemistry, Tufts University School of Medicine, Boston, Massachusetts 02111, and Department of Biochemistry, University of Massachusetts School of Medicine, Shrewsbury, Massachusetts 01545

Received June 1, 2000; Revised Manuscript Received September 19, 2000

ABSTRACT: Skeletal muscle troponin C (TnC) adopts an extended conformation when crystallized alone and a compact one when crystallized with an N-terminal troponin I (TnI) peptide, TnI_{1-47} [Vassylyev et al. (1998) *Proc. Natl. Acad. Sci. U.S.A. 95*, 4847−4852]. The N-terminal region of TnI (residues 1−40) was suggested to play a functional role of facilitating the movement of TnI's inhibitory region between TnC and actin [Tripet et al. (1997) *J. Mol. Biol. 271*, 728−750]. To test this hypothesis and to investigate the conformation of TnC in the intact troponin complex and in solution, we attached fluorescence and photo-cross-linking probes to a mutant TnI with a single cysteine at residue 6. Distances from this residue to residues of TnC were measured by the fluorescence resonance energy transfer technique, and the sites of photo-cross-linking in TnC were determined by microsequencing and mass spectrometry following enzymatic digestions. Our results show that in the troponin complex neither the distance between TnI residue 6 and TnC residue 89 nor the photo-cross-linking site in TnC, Ser133, changes with Ca^{2+}, in support of the notion that this region plays mainly a structural rather than a regulatory role. The distances to residues 12 and 41 in TnC's N-domain are both considerably longer than those predicted by the crystal structure of TnC·TnI_{1-47}, supporting an extended rather than a compact conformation of TnC. In the binary TnC·TnI complex and the presence of Ca^{2+}, Met43 in TnC's N-domain was identified as the photo-cross-linking site, and multiple distances between TnI residue 6 and TnC residue 41 were detected. This was taken to indicate increased flexibility in TnC's central helix and that TnC dynamically changes between a compact and an extended conformation when troponin T (TnT) is absent. Our results further emphasize the difference between the binary TnC·TnI and the ternary troponin complexes and the importance of using intact proteins in the study of structure−function relationships of troponin.

Striated (skeletal and cardiac) muscle is regulated by the intracellular Ca^{2+} concentration via the thin filament complex, troponin (Tn). Of the three Tn subunits, troponin C (TnC) plays the role of the Ca^{2+} receptor; troponin I (TnI), the inhibitory subunit, switches between TnC and actin; and troponin T (TnT), the Tm-binding subunit, anchors TnC and TnI on the Tm·F-actin filament. It is currently thought that in the absence of Ca^{2+} the actin-binding regions in the C-terminal portion of TnI are bound to actin, resulting in the inhibition of active cyclic interaction between myosin cross-bridges and actin. In response to Ca^{2+} binding to the N-domain of TnC, the actin-binding regions of TnI detach from actin, allowing the activation of acto-myosin interaction and contraction (*1*, *2*).

TnC has been crystallized and its structure has been solved in both the $2Ca^{2+}$ (*3*, *4*) and $4Ca^{2+}$ (*5*, *6*) states. The largely α-helical TnC molecule has two globular domains, the N-

† This work was supported by National Institutes of Health Grant AR21673.

* To whom correspondence should be addressed at Boston Biomedical Research Institute, 64 Grove St., Watertown, MA 02472. Telephone 617-658-7807; fax 617-972-1753; e-mail tao@bbri.org.

‡ Boston Biomedical Research Institute.

§ University of Massachusetts School of Medicine.

|| Massachusetts General Hospital

⊥ Department of Biological Chemistry and Molecular Pharmacology, Harvard Medical School.

Department of Neurology, Harvard Medical School

◇ Tufts University School of Medicine.

[1] Abbreviations: Tn, troponin; TnC, troponin C; TnI, troponin I; TnT, troponin T; Tm, tropomyosin; TnI6, recombinant troponin I with a single cysteine at residue 6; TnC12, TnC41, and TnC89, recombinant troponin C with single cysteines at residues 12, 41, and 89, respectively; BP-IA, benzophenone-4-iodoacetamide; $I6^{BP}$, troponin I with benzophenone attached to the single cysteine at residue 6; I6−C, photo-cross-linking product of troponin I with benzophenone attached to the single cysteine at residue 6 with troponin C; 1,5-IAEDANS, *N*-iodoacetyl-N′-(5-sulfo-1-naphthyl)ethylenediamine, and DAN, dansyl moiety of 1,5-IAEDANS; DAB-Mal, [4-(dimethylamino)phenyl]-azophenyl-4′-maleimide, and DAB, [(dimethylamino)phenyl]azophenyl moiety of DAB-Mal; DDP-Mal, *N*-[4-(dimethylamino)-3,5-dinitrophenyl]maleimide, and DDP, (dimethylamino) dinitrophenyl moiety of DDP-Mal; $I6^{DAN}$ and $C12^{DAB}$, examples of troponin I and C mutants with probes labeled at their single cysteines; *R*(I6−C12), *R*(I6−C41), and *R*(I6−C89), distances between troponin I residue 6 and troponin C residues 12, 41, and 89, respectively; DTT, dithiothreitol; EDTA, ethylenediaminetetraacetic acid; EGTA, ethylene glycol bis(β-aminoethyl ether)-*N*,*N*,*N*′,*N*′-tetraacetic acid; HEPES, *N*-(2-hydroxyethyl)-piperazine-*N*′-(2-ethanesulfonic acid); Tris, tris(hydroxymethyl)-aminomethane; HPLC, high-performance liquid chromatography; FRET, fluorescence-detected resonance energy transfer; MALDI-TOF, matrix-assisted laser desorption/ionization time-of-flight mass spectrometry; MH^+, mass of singly protonated peptides; SDS−PAGE, sodium dodecyl sulfate−polyacrylamide gel electrophoresis.

10.1021/bi001259x CCC: $19.00 © 2000 American Chemical Society
Published on Web 11/21/2000

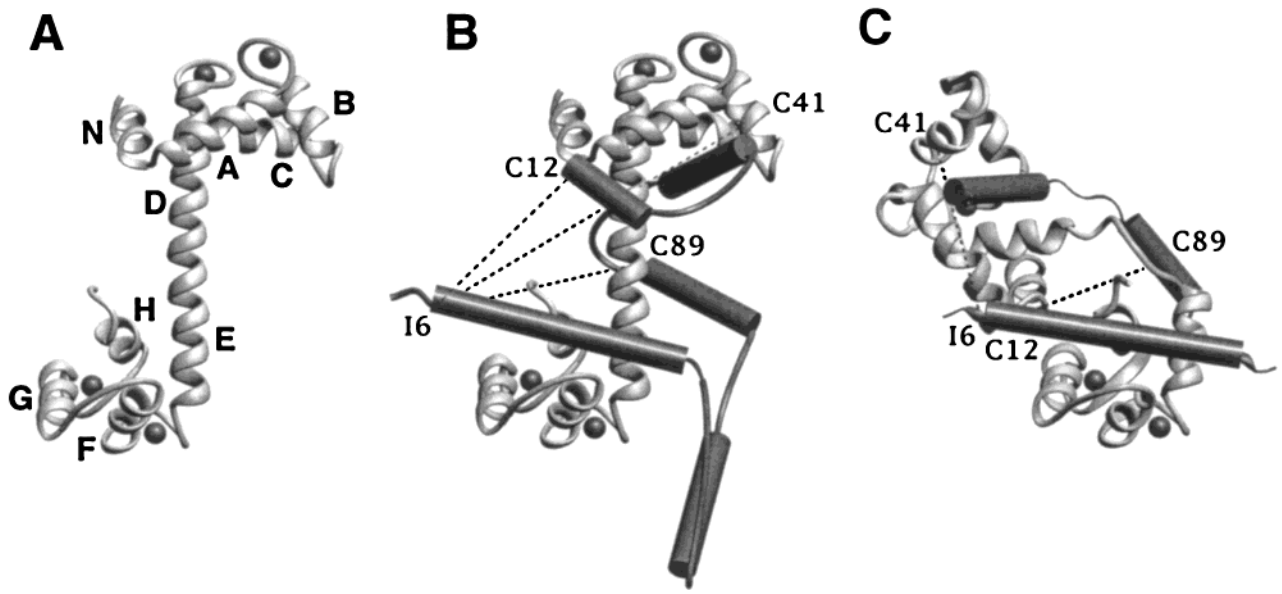

FIGURE 1: Crystal structure of TnC (A) (*5*) and comparison of the "extended" (B) and the "compact" (C) models of TnC and TnI, taken from the models of Luo et al. (*12*) and of Vassylyev et al. (*13*), respectively. Barrels are predicted helical segments of TnI. The helices of TnC and the positions of TnI residue 6 and of TnC residues 89, 41, and 12 are labeled.

and C-domains, linked by a long central helix composed of helices D and E (Figure 1A). The major difference between the two structures is the conformation of the hydrophobic cleft in the N-domain. It is closed in the $2Ca^{2+}$ state and open in the $4Ca^{2+}$ state, exposing a patch of hydrophobic residues. The central role of this conformational change in transmitting the Ca^{2+}-binding signal from TnC to TnI was proposed by Herzberg et al. (*7*) and supported by mutagenesis experiments showing that mutations inhibiting this transition impair TnC's regulatory function (*8*). Biochemical (*9*) and NMR (*10*) studies showed that peptides containing residues 96−148 interact with TnC's N-domain cleft. Our photo-cross-linking study on intact Tn identified Met121 in the triggering region (residues 114−137) to be in TnC's N-domain cleft (*11, 12*).

The antiparallel arrangement of TnI and TnC is now well established (for a review see ref *2*). The crystal structure of TnC complexed with an N-terminal peptide of TnI, TnI_{1-47} (*13*), shows that TnI residues 3−33 forms an α-helix and the segment 13−30 binds to the C-domain cleft of TnC. There are also reports that the inhibitory region of TnI, residues 96−116, interacts with the C-domain of TnC (*9, 14*). It was proposed that in the presence of Ca^{2+} the inhibitory region is bound to TnC's C-domain cleft and that, upon Ca^{2+} removal, TnI's N-terminal region displaces the inhibitory region from TnC's C-domain cleft, thereby playing the functional role of assisting the movement of the inhibitory region (*9*). This mechanism still needs to be verified with intact protein complexes. By combination of information derived from a wide variety of studies, a model for the conformations of TnI and TnC in the Tn complex was proposed (*12*): in the presence of Ca^{2+}, TnI's residues 1−33 interact with TnC's C-domain cleft; residues 48−89, with TnT; residues 90−113, with TnC's central helix; residues 114−125, with TnC's N-domain cleft; and residues 130−150, with TnC's A-helix (Figure 1B). In the absence of Ca^{2+}, TnI residues 114−125 (triggering region) move out of TnC's N-domain cleft and trigger the movements of residues 90−113 (inhibitory region) and 130−150 toward actin.

A surprising aspect of the above-mentioned $TnC{\cdot}TnI_{1-47}$ crystal structure is the unwinding and bending of TnC's central helix at the D−E helices junction, causing the two TnC globular domains to be much closer to each other (*13*), perhaps as a consequence of the peptide's N-terminus being in contact with TnC's A-helix in the N-domain. On the basis of this finding and sequence homology between TnI residues 17−27 and 117−127, a partial structural model for the TnC·TnI complex was proposed (*13*) (Figure 1C). It is not clear whether this represents a stable or a dynamic intermediate conformation of the Tn complex in solution and whether this folding has any functional implications. Two low-angle neutron scattering studies concluded that TnC is extended in the binary TnC·TnI (*15*) and in the ternary Tn complex (*16*).

In this work we examined both the folding of TnC and the proposed competition between the inhibitory and N-terminal TnI regions for TnC's C-domain cleft in the intact Tn complex. This was done by studying the proximity of TnI's N-terminus relative to both the C- and N-domains of TnC. For this purpose we constructed a mutant rabbit skeletal TnI that contains a single cysteine at residue 6, to which either a photo-cross-linker or a fluorescence probe could be attached for determination of photo-cross-linking sites in TnC and measurements of distances to TnC residues. Residue 6 of TnI was chosen for the following reasons: (1) It was shown in the crystal structure of $TnC{\cdot}TnI_{1-47}$ not to be directly involved in the binding of the N-terminal region of TnI with TnC's C-domain cleft. Therefore, the attachment of probes at this residue is unlikely to interfere with the binding. (2) Our previous work showed that this TnI residue could be photo-cross-linked to TnC with very high yield in both the binary TnC·TnI and the ternary Tn complex and in both the $4Ca^{2+}$ and $2Mg^{2+}$ states (*12*). This facilitated the purification of the cross-linking products for analyzing the cross-linking sites in TnC by successive proteolysis, sequence analysis, and mass spectrometry. (3) As can be seen in Figure 1 and Table 2, distances from this residue to some residues in TnC's N-domain are very sensitive to the conformation

of TnC's central helix. For example, the distance to residue 12 is ~13 Å in the structure of TnC·TnI_{1-47} (*13*) and ~30 Å in the model of TnC·TnI with extended TnC central helix (*12*). Measuring the distances between TnI residue 6 and various TnC residues in the intact Tn complex would therefore provide direct information on the conformation of the complex.

Both our distance measurements and photo-cross-linking results reported here support the view that in the intact Tn complex TnC adopts an extended conformation, and TnI's N-terminal region associates with TnC's C-domain in both the presence and the absence of Ca^{2+}. However, in the binary TnC·TnI complex some variability in TnC's conformation, possibly owing to some flexibility in the central helix could be observed.

MATERIALS AND METHODS

Chemicals. Common reagents of the highest grade were from Sigma or Aldrich. HEPES was from Research Organics (Cleveland, OH); BP-Mal, DAB-Mal, and DDP-Mal were from Molecular Probes (Eugene, OR); and 1,5-IAEDANS was from Sigma. Materials for recombinant DNA procedures were from New England Biolabs (Beverly, MA) and U.S. Biochemical Corp. (Cleveland, OH); materials for SDS−PAGE were from Bio-Rad (Hercules, CA); and the BCA protein assay was from Pierce (Rockford, IL).

Protein Preparations. Wild-type Tn subunits were purified from rabbit skeletal muscle according to established methods (*17*). A single-cysteine mutant of TnI, TnI6, was constructed by converting the endogenous cysteines, Cys48, Cys64, and Cys133, to serines and Arg6 to cysteine by previously described mutagenesis, expression, and purification procedures (*18*). Single-cysteine mutants of TnC, TnC12, TnC41, and TnC89, were constructed by converting the endogenous Cys98 to leucine and either Ser12 or Thr41 or Gly89 to cysteine by published procedures (*19*). Purity of prepared proteins was assessed by SDS−PAGE.

Labeling of single-cysteine TnI and TnC mutants was carried out in denaturing solution containing 4 M guanidine hydrochloride, 20 mM HEPES, pH 7.5, 0.1 M NaCl, and 2 mM EDTA with ~40 μM protein and 200 μM probe. The time and temperature for incubation were varied to maximize the labeling efficiency with a maximum of 3 h at 22 °C followed by overnight at 4 °C. The alkylation reactions were quenched by 10 mM DTT, and the unreacted probes were removed by dialysis against the same buffer. The following extinction coefficients were used to determine the concentrations of proteins and probes: $\epsilon_{280} = 0.18$ and 0.4 $(mg/mL)^{-1}$ cm^{-1} for TnC and TnI, respectively; $\epsilon_{280} = 13\,000$ M^{-1} cm^{-1} for BP-Mal; $\epsilon_{337} = 6000$ M^{-1} cm^{-1} and $\epsilon_{280} = 1060$ M^{-1} cm^{-1} for 1,5-IAEDANS; $\epsilon_{460} = 24\,800$ M^{-1} cm^{-1} and $\epsilon_{280} = 8400$ M^{-1} cm^{-1} for DAB-Mal; and $\epsilon_{440} = 2620$ M^{-1} cm^{-1} for DDP-Mal. In the case of labeling TnI6 with BP-Mal, the BCA protein assay was performed to determine the protein concentration with unlabeled TnI as standard.

The binary TnC·TnI and the ternary Tn complexes were reconstituted by mixing labeled or unlabeled TnC and TnI, or TnC, TnI, and TnT, in the above denaturing solutions at equimolar ratio. The mixtures were then dialyzed against a solution containing 10 mM HEPES, pH 7.5, 0.1 M NaCl, 0.2 mM $CaCl_2$, and 0.2 mM DTT. After centrifugation to remove any insoluble TnI or TnT, the samples were subjected to SDS−PAGE alongside with purified rabbit skeletal Tn. The extent of reconstitution was checked by comparing the staining intensities of the subunits derived from the reconstituted samples with those from the purified Tn.

Resonance Energy Transfer. The fluoresence decay curves for the fluorescent donor 1,5-IAEDANS attached to TnI6 or one of the TnC mutants were obtained in the absence and the presence of a nonfluorescent acceptor, DAB-Mal or DDP-Mal, by use of a photon-counting nanosecond fluorometer (*20*). The donor fluorescence lifetimes in the absence and the presence of an acceptor, τ_d and τ_{da}, respectively, were determined from the corresponding decay curves by the method-of-moments (MOM) with the program FLUOR (*21*). The interprobe distance R was then calculated according to Förster's equations (*22*):

$$E = 1 - \tau_{da}/\tau_d \quad (1)$$

where E is the transfer efficiency and R_0 is the critical transfer

$$R = R_0(E^{-1} - 1)^{1/6} \quad (2)$$

distance that is corrected for the variation in donor fluorescence quantum yield by use of the relation $R_0 = R_0'(\tau_d/\tau_d')^{1/6}$; $R_0' = 39.9$ Å and $\tau_d' = 13.5$ ns for the DAN−DAB pair (*23*), and $R_0' = 29$ Å and $\tau_d' = 20.6$ ns for the DAN−DDP pair (*24*).

DAB-Mal attached to TnI6 was used as the acceptor in preliminary measurements of all three distances. Reasonable lifetimes were obtained for the $I6^{DAB}$·$C12^{DAN}$ and the $I6^{DAB}$·$C41^{DAN}$ pairs, indicating that DAB-Mal is a suitable acceptor for measuring the distances from TnI residue 6 to these two TnC positions. For the $I6^{DAB}$·$C89^{DAN}$ pair, however, a very short lifetime (~2 ns) was obtained, indicating that the distance from TnI residue 6 to TnC residue 89 is too short to be measured reliably with DAB-Mal. Therefore, DDP-Mal was used as the acceptor in subsequent measurements of this distance.

Photo-Cross-Linking and Identification of the Cross-Linking Sites. Photo-cross-linking reactions of BP-IA-labeled TnI6 in the TnC·TnI and Tn complexes were induced by UV irradiation in borosilicate glass tubes for 25 min in the cold room. For each complex the reaction was carried out in the $4Ca^{2+}$ and $2Mg^{2+}$ states. The previously observed high-yield cross-linking of TnI6 to TnC under all these conditions (Figure 2 in ref *12*) was reproduced. The cross-linking products were purified as follows: the irradiated binary complexes were filtered with 0.22 μm filters and loaded onto a Mono Q anion-exchange column (Pharmacia) preequilibrated with a buffer containing 6 M urea, 20 mM Tris-HCl (pH 8.0), 0.1 M NaCl, 4 mM EDTA, and 2 mM DTT. The samples were fractionated by FPLC (Waters 6) with a salt gradient up to 0.6 M NaCl in the same buffer. The irradiated ternary complexes were dialyzed against H_2O containing 0.1% TFA and fractionated with a C_8 analytical column (Vydac) on HPLC (Beckman) with gradients of acetonitrile up to 99.9%. The slopes were varied to achieve the best separation, and multiple runs were performed to accommodate the capacities of the columns. The purified products were dialyzed against H_2O and lyophilized before further analysis.

Tryptic Cleavage. Purified complexes were dissolved in 25 μL of a 8 M urea and 100 mM ammonium bicarbonate solution and then diluted with water to make the final urea concentration 2 M. One microgram of trypsin (Promega) in 4 μL of 50 mM acetic acid was then added and the sample was incubated at 37 °C overnight. The final ratio of enzyme: substrate was ~1:50 by weight. Tryptic peptides were separated on a 2.1 mm × 25 cm Vydac (218TP52) C_{18} column with a linear gradient from 100% solvent A (0.1% TFA) to 70% solvent B [0.08% TFA in acetonitrile/water (70/30)] in 70 min at a flow rate of 210 μL/min. The eluate was monitored with a Hewlett-Packard UV diode-array detector at 210 and 260 nm for polypeptides and the BP moiety, respectively; fractions were collected manually.

Endoproteinase Asp N Cleavage. The cross-linked fraction found at 64′ in the tryptic digests of the TnI6−TnC (photolyzed in the ternary Tn complex in the $4Ca^{2+}$ or $2Mg^{2+}$ state) were further digested with endoproteinase Asp N (Boehringer Mannheim) under the same conditions as for the tryptic digestions described above. Fractions were dried to near completion and taken up in the digestion buffer containing 100 mM ammonium bicarbonate, 1% *n*-octyl glucoside, and 10% acetonitrile. Asp N peptides were separated on a 0.5 mm × 150 mm C_{18} column (Brownlee) with a linear gradient from 100% solvent A to 70% solvent B in 70 min at a flow of 210 μL/min. Eluates were again monitored at 210 and 260 nm and fractions were collected manually.

Protein Sequencing, Mass Spectrometry, and HPLC. Automated Edman degradations were performed on a Applied Biosystems/Perkin-Elmer 494 Procise sequencing system. MALDI-TOF mass spectrometry was performed on a PerSeptive Biosystems linear Voyager BioSpectrometry Workstation with α cyano-4-hydroxycinnamic acid as the matrix. HPLC was performed on a Hewlett-Packard 1090 M HPLC system equipped with an UV photodiode-array detector.

RESULTS

Distances from TnI Residue 6 to TnC Residues. We used FRET to measure the distances from TnI residue 6 to TnC residues 12, 41, and 89, *R*(I6−C12), *R*(I6−C41), and *R*(I6−C89), respectively. 1,5-IAEDANS was used as the donor and either DAB-Mal or DDP-Mal was used as acceptor. It was shown previously that neither the mutations nor the labeling affected the activities of TnI and TnC (*12*, *25*). Each measurement was made in the $4Ca^{2+}$ state (0.2 mM $CaCl_2$, saturating all four metal binding sites in TnC), simulating the physiological activated state, and in the $2Mg^{2+}$ state (2 mM EGTA, 8 mM $MgCl_2$, saturating only the C-domain sites of TnC), simulating the physiological inhibited or relaxed state. Rabbit skeletal proteins were used throughout.

The procedures for analyzing the decay curves and calculating distances follow closely those described in Luo et al. (*18*). Here we briefly describe them for one data set as an example. The decay curve of $I6^{DAN}$·C12 in the $4Ca^{2+}$ state (Figure 2, upper curve) appears linear in the semilogarithmic plot, indicating a single-exponential decay. MOM analysis yielded a lifetime of 14.46 ns (Table 1), which was taken as τ_d, the donor lifetime in the absence of acceptor. The decay of $I6^{DAN}$·$C12^{DAB}$ (Figure 2, lower curve) is apparently

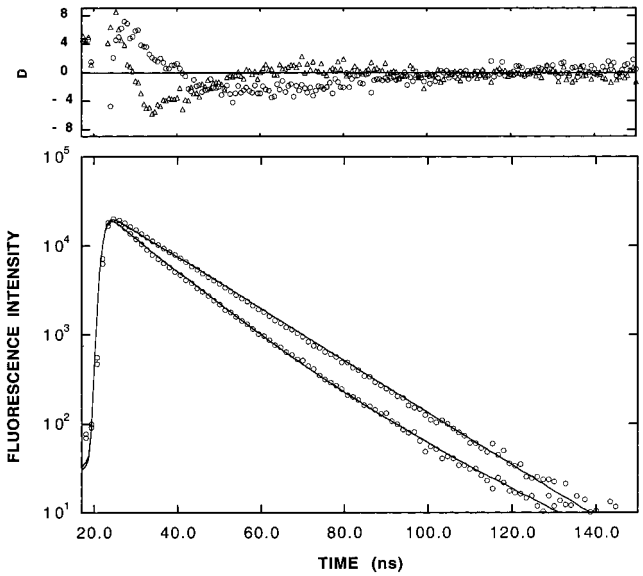

FIGURE 2: Fluorescence decay curves of $I6^{DAN}$·C12 (upper curve) and $I6^{DAN}$·$C12^{DAB}$ (lower curve). Circles are experimental points, of which every other is shown. Solid lines are calculated curves with parameters derived from MOM analyses (Table 1). Upper panel: the deviation functions for $I6^{DAN}$·C12 (○) and $I6^{DAN}$·$C12^{DAB}$ (△) decay curves. The deviation function is defined as $D_i = (c_i - e_i)/(e_i)^{1/2}$, where c_i and e_i are the calculated and experimental fluorescence intensities, respectively, at the *i*th data point. All measurements were made at 20 °C.

multiexponential. Triexponential MOM analysis yielded two components whose lifetimes (16.37 and 9.78 ns) are similar to those derived from biexponential analysis (23.07 and 10.34 ns) and a third components whose lifetime (46.12 ns) is too long to be physical and whose fractional amplitude (0.001) is negligibly small. This indicates that the decay is essentially biexponential, with the long lifetime corresponding to the unquenched lifetime of donor moieties that are not paired with acceptors and the short lifetime corresponding to the quenched lifetime. This was taken as τ_{da}, the donor lifetime in the presence of acceptor. Substituting the values of τ_d and τ_{da} into eqs 1 and 2, we obtained $R = 45.6$ Å. Note that use of the quenched lifetime derived from biexponential analysis (10.34 ns) as τ_{da} yielded a very similar value for *R* (47.6 Å). The error for this kind of measurements is 1−2 Å, assessed in a previous study in which repetitive measurements were made (*18*).

The data for all the samples were analyzed as described above, and the results are summarized in Table 1. For brevity, we listed only results from monoexponential analysis for donor-alone decay and triexponential analysis for donor−acceptor decay unless the results contain negative parameters (lifetime or fractional amplitude). In such cases the biexponential analysis results were listed. All the donor−acceptor decays are clearly biexponential with the exception of that for $I6^{DAN}$·$C41^{DAB}$ in the $4Ca^{2+}$ state. In this case, aside from an unquenched component and a major quenched component of τ =10.30 ns and fractional amplitude of 0.837, a third component of τ =2.72 ns with a significant fractional amplitude of 0.112 was obtained. This more complicated decay behavior may reflect a more dynamic spatial relationship between the probes on the two proteins. The two distances calculated from the two quenched lifetimes, 47.0 and 31.6 Å, are taken to indicate the range of interprobe distances. Table 2 shows all the measured distances, along

Table 1: Parameters of Fluorescence Decay and RET between TnI Residue 6 and Select TnC Residues in $4Ca^{2+}$ and $2Mg^{2+}$ States

sample	state	τ_1 (A_1)[a]	τ_2 (A_2)	τ_3 (A_3)	E	R_0	R	χ^2/N[b]
$I6^{DAN}$·C	4Ca	14.46 (1.00)						3.5
$I6^{DAN}$·$C12^{DAB}$	4Ca	16.37 (0.181)	9.78 (0.817)	46.12 (0.001)	0.323	40.36	45.6	3.4
$I6^{DAN}$·$C41^{DAB}$	4Ca	18.57 (0.051)	10.30 (0.837)	2.72 (0.112)		40.36	31.6,[c] 47.0[d]	0.8
$I6^{DAN}$·$C89^{DDP}$	4Ca	11.79 (0.997)	33.04 (0.003)			27.34	35.0	3.0
$I6^{DAN}$·C	2Mg	13.83 (1.00)						1.8
$I6^{DAN}$·$C12^{DAB}$	2Mg	16.61 (0.291)	10.47 (0.709)			40.04	48.4	1.3
$I6^{DAN}$·$C41^{DAB}$	2Mg	17.31 (0.184)	11.07 (0.815)	48.90 (0.001)	0.198	40.04	50.6	4.2
$I6^{DAN}$·$C89^{DDP}$	2Mg	19.26 (0.057)	12.82 (0.943)			27.12	41.5	1.6
$I6^{DAN}$·C·T	4Ca	14.38 (1.00)						2.9
$I6^{DAN}$·$C12^{DAB}$·T	4Ca	16.69 (0.244)	9.31 (0.755)	49.71 (0.001)	0.352	40.32	44.6	3.5
$I6^{DAN}$·$C41^{DAB}$·T	4Ca	16.89 (0.108)	10.77 (0.892)	58.8 (0.001)	0.251	40.32	48.4	3.9
$I6^{DAN}$·$C89^{DDP}$·T	4Ca	24.64 (0.021)	11.87 (0.977)	49.05 (0.001)	0.175	27.31	35.4	3.2
$I6^{DAN}$·C·T	2Mg	14.25 (1.00)						2.5
$I6^{DAN}$·$C12^{DAB}$·T	2Mg	13.43 (0.635)	5.35 (0.359)	34.53 (0.005)		40.23	37.0	1.3
$I6^{DAN}$·$C41^{DAB}$·T	2Mg	15.72 (0.259)	10.10 (0.741)	46.60 (0.001)	0.288	40.23	46.8	1.5
$I6^{DAN}$·$C89^{DDP}$·T	2Mg	16.49 (0.375)	9.46 (0.625)			27.25	30.6	1.7

[a] τ is the fluorescence decay lifetime in nanoseconds, and A is the fractional amplitude of each decay component. [b] χ^2/N is the mean residual, defined as $\Sigma_1^N[(f_I - f_{ci})^2/f_I]/N$, where N is the number of data points, f_i is the measured intensity of the ith data point, and f_{ci} is the calculated intensity from the derived parameters. [c] Distance calculated with τ_3. [d] Distance calculated with τ_2.

Table 2: Measured and Calculated Distances from TnI Residue 6 to TnC Residues in the N- and C-Domains

probe location	state	measured distances (Å)		calculated distances (Å)	
		binary[a]	ternary[b]	extended[c]	compact[d]
I6−C12	4Ca	45.6	44.6	32.0	12.9
	2Mg	48.4	37.0	31.1	13.9
I6−C41	4Ca	31.6−47.0	48.4	55.6	31.1
	2Mg	50.6	46.8	47.8	22.3
I6−C89	4Ca	35.0	35.4	31.4	25.4
	2Mg	41.5	30.6	31.6	25.6

[a] Measurements were made in the TnI·TnC binary complexes. [b] Measurements were made in the TnI·TnC·TnT ternary complexes. [c] The models used for the $4Ca^{2+}$ and $2Mg^{2+}$ states are Figure 10 panels A and B, respectively, in ref *12*. [d] The models used for the $4Ca^{2+}$ and $2Mg^{2+}$ states are the crystal structure and the modeled structure, respectively, in ref *13*.

with calculated distances based on an "extended" or a "compact" model (see Discussion).

Photo-Cross-Linking Sites on TnC. The tryptic digest (see Materials and Methods) of irradiated $I6^{BP}$·C in the $4Ca^{2+}$ state had a peak eluting at 30 min with absorbance at both 210 and 260 nm (Figure 3A) that was previously identified as a tryptophan-containing C-terminal TnI tryptic peptide (see Figure 3 in ref *11*). Another peak eluting at 36 min that absorbed strongly at 260 nm was found to contain a single peptide with MH^+ of 1434 Da by MALDI mass spectrometry (Figure 3B). Sequence analysis showed that this peptide contained the expected TnI tryptic fragment XNR (residues 6−8), where X denotes the modified Cys6 that showed no phenylthiohydantoin (PTH) derivative in the analysis. It is in 1:1 molar ratio with residues ELGTVxR, corresponding to TnC residues 38−44 where Met43 (denoted by x) was not detectable, indicating that this is the site of cross-linking. The calculated mass of 1433 Da (390 Da for TnI residues 6−8, 805 Da for TnC residues 38−44, and 238 Da for the cross-linker) agrees well with the mass spectrometric data supporting this assignment.

The digestion patterns for irradiated $I6^{BP}$·C in the $2Mg^{2+}$ state and $I6^{BP}$·C·T in the $4Ca^{2+}$ and $2Mg^{2+}$ states are almost identical but very different from the one above. The major peak that absorbs strongly at 260 nm was eluted at 64 min (Figure 4A). For all three samples, mass spectrometric analysis of this fraction showed a large fragment with MH^+ of 8775 Da (Figure 4B). Sequence analyses again yielded the expected TnI residues (XNR). The identifiable TnC residues were GKSEEELAE, corresponding to a fragment starts from residue 89. The mass of this TnC fragment could be calculated to be 8147 Da (8775 − 390 − 238 Da), suggesting that the fragment corresponds to TnC residues 89−159, whose calculated mass is 8150 Da.

To identify the exact cross-linking site in this large TnC C-terminal fragment, the 64 min fractions from the ternary complex samples were further digested with endoproteinase Asp N. The HPLC elution profiles were identical, with two peaks at 30 and 32 min that showed high A_{260} (Figure 5A). Sequence analysis for both fractions from both samples yielded the same expected TnI residues (XNR) in 1:1 molar ratio to TnC residues 128−136 DEEIExLMK. Ser133 (designated as x) was in very low yield, indicating that it is modified by the cross-linking. Mass spectrometric analyses for the two peaks (30 and 32 min) yielded a single peptide with MH^+ of 1722.65 Da (Figure 5B). It is curious that two well-separated fractions showed the same mass by MALDI-MS. It is possible that the distinguishing characteristic was removed by the ionization process. The mass of the TnC peptide could be obtained from the total mass minus the mass of the TnI peptide and that of the cross-linker (1722.65 − 390.44 − 238 = 1094.21 Da). This agrees very well with the calculated mass of TnC residues 128−136 (1093.21 Da), in support of our assignment.

We therefore conclude that, in the ternary Tn complex, residue 6 of TnI cross-links to a C-terminal residue of TnC, Ser133, regardless of Ca^{2+}. However, in the TnI·TnC binary complex the cross-linking site on TnC becomes Ca^{2+}-dependent, being at Ser133 in the $2Mg^{2+}$ state and Met43 in the $4Ca^{2+}$ state. Note that although the sites of cross-linking and interaction are expected to be close to each other, they may not be exactly the same because of the ~9 Å span of the BP photo-cross-linker.

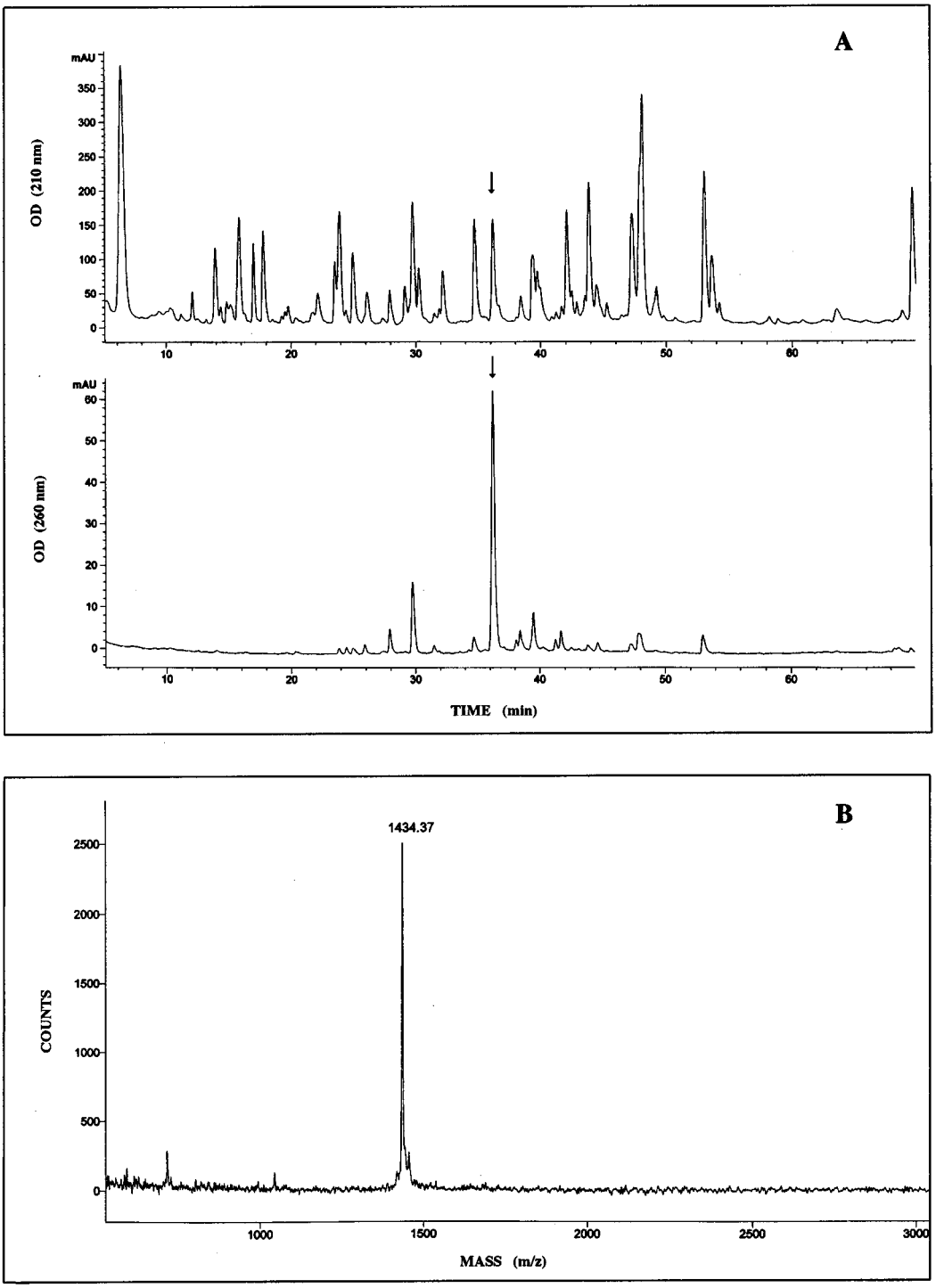

FIGURE 3: (A) Reverse-phase HPLC separation of tryptic digest of irradiated $I6^{BP}$•C in the $4Ca^{2+}$ state monitored at 210 nm (upper) and 260 nm (lower). The elution positions of the cross-linked peptides are indicated by arrows. (B) MALDI-TOF mass spectrum for the cross-linked peptide. The mass of the peptide in the fraction that eluted at 36 min in panel A was determined by mass spectrometry. The mass of 1434.37 Da represent singly protonated cross-linked peptides.

DISCUSSION

This work addresses three questions: first, several studies had suggested that peptides corresponding to the N-terminal region of TnI (first ~40 residues) interact with TnC's C-domain (*26*−*28*). The recent crystal structure of TnC•TnI_{1-47} (*13*) shows that the peptide binds at TnC's C-domain cleft. The question that arises is whether the same structure is obtained in complexes composed of full-length proteins and in solution. Second, the crystal structure of TnC•TnI_{1-47} (*13*) demonstrated the possibility that TnC's central helix can be unfolded and bent, resulting in a more compact conformation reminiscent of calmodulin (*29*) and myosin light chains (*30*) in complex with their target proteins. The question is whether in the intact complexes TnC adopts this compact conformation or an extended one as in the crystal structure of free TnC. Third, on the basis of studies with peptides corresponding to TnI's N-terminal and inhibitory regions, it was proposed that in the presence of Ca^{2+} the inhibitory region is bound to TnC's C-domain cleft, and upon Ca^{2+} removal the N-terminal region displaces the inhibitory region from

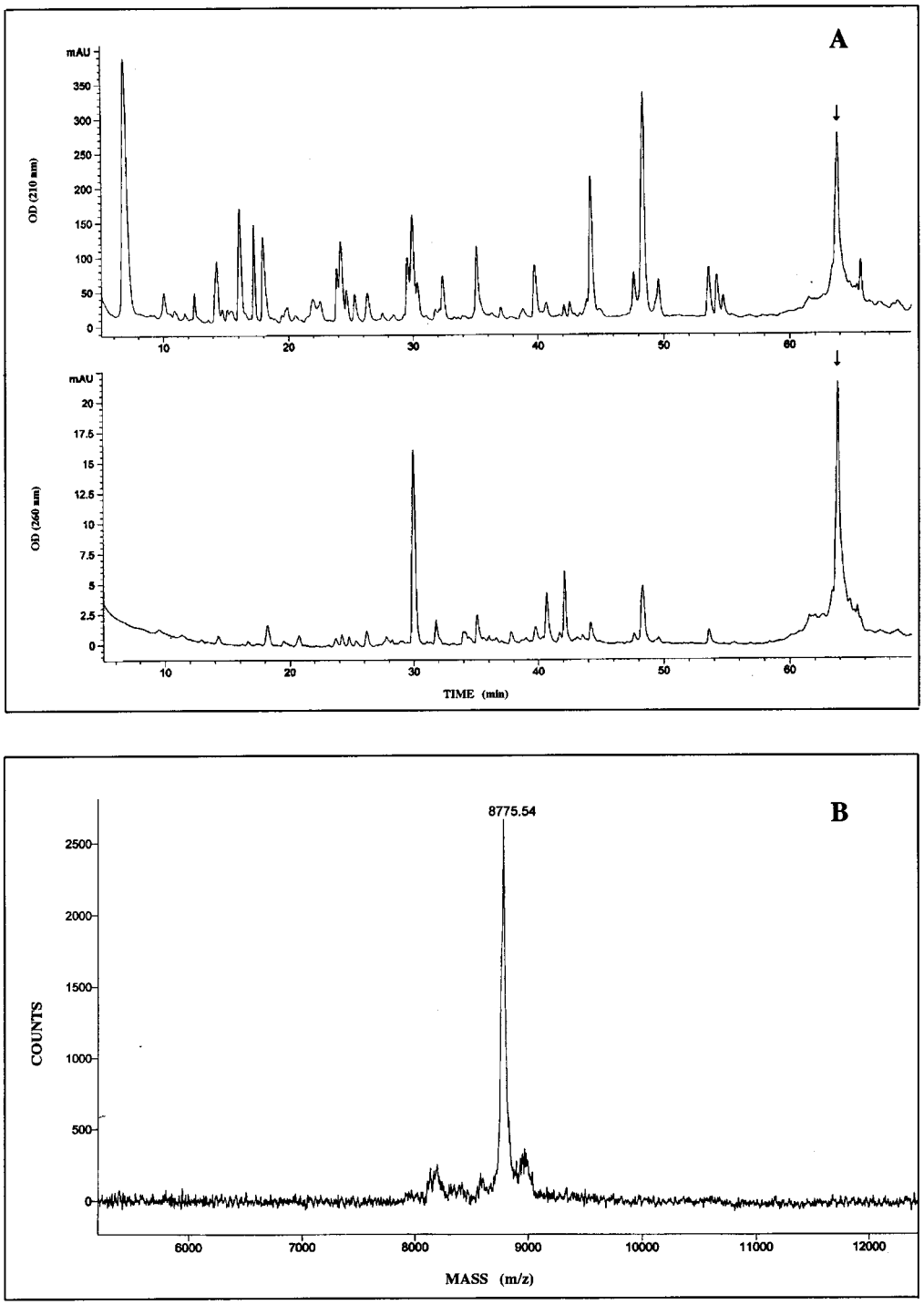

FIGURE 4: (A) Reverse-phase HPLC separation of tryptic digests of irradiated $I6^{BP}$·C in the $2Mg^{2+}$ state and $I6^{BP}$·C·T in the $4Ca^{2+}$ and $2Mg^{2+}$ states monitored at 210 nm (upper) and 260 nm (lower). Others are the same as in Figure 3A. (B) MALDI-TOF mass spectrum for the cross-linked peptide. The mass of the peptide in the fraction that eluted at 64 min in panel A was determined by mass spectrometry. The mass of 8775.54 Da represent singly protonated cross-linked peptides.

TnC's C-domain cleft, thereby facilitating the movement of the inhibitory region toward actin (*9*, *26*). The question is whether this occurs in the intact system.

Binding of TnI's N-Terminal Region to TnC's C-Domain. Previously we showed that $I6^{BP}$ photo-cross-links to TnC in both TnI·TnC and Tn and in both the $4Ca^{2+}$ and the $2Mg^{2+}$ states (Figure 2 in ref *12*). In this work we isolated the cross-linked complexes and identified the photo-cross-linking sites in TnC. In the ternary Tn complex $I6^{BP}$ cross-links to a C-terminal TnC residue, Ser133, in both the $4Ca^{2+}$ and the $2Mg^{2+}$ states. This indicates that TnI residue 6 is within ~10 Å, the span of the benzophenone cross-linker, of TnC Ser133. The α-carbon of TnC Ser133 is 13 Å from that of TnI residue 6 in the crystal structure of the TnC·TnI_{1-47} complex (*13*). Our results therefore support the notion that in solution and in the intact Tn complex TnI's N-terminal region is bound to TnC's C-domain cleft as in the crystal structure of TnC·TnI_{1-47} (*13*). Moreover, neither the yield (*12*) nor the site (this work) of cross-linking was Ca^{2+}-dependent. Our results therefore argue against the hypothesis that TnI's N-terminal region is displaced from TnC's C-domain cleft by the inhibitory region in the $2Mg^{2+}$ state (*9*, *26*). Recent

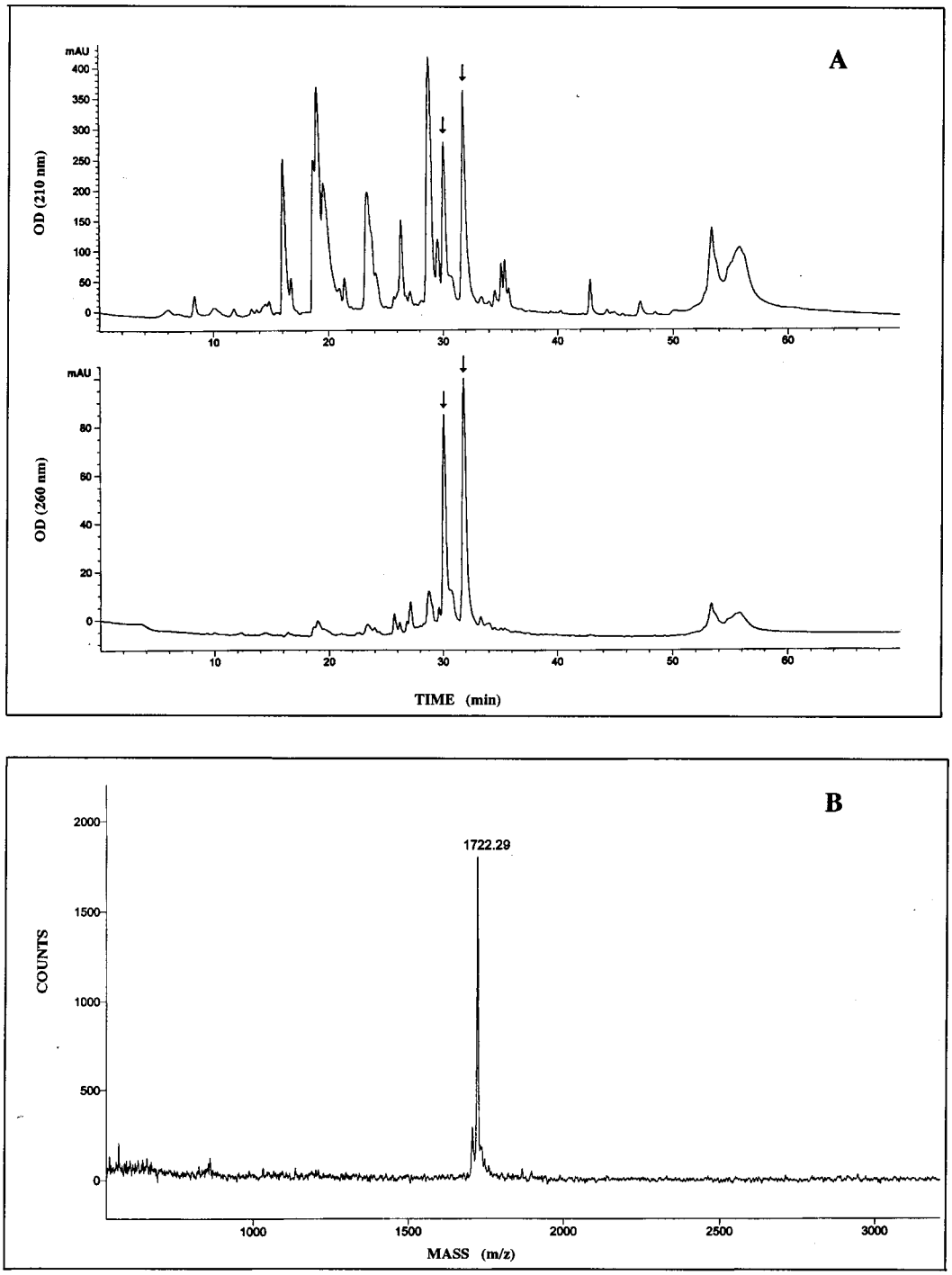

FIGURE 5: (A) Reverse-phase HPLC separation of endoproteinase Asp N digests. The 64 min fractions in the tryptic digests of irradiated $I6^{BP}$•C•T in the $4Ca^{2+}$ and $2Mg^{2+}$ states (see Figure 4A) were further digested with endoproteinase Asp N. The HPLC separations were monitored at 210 nm (upper) and 260 nm (lower). The arrows indicate fractions containing cross-linked peptides. (B) MALDI-TOF mass spectra for the cross-linked peptide. The mass of the peptides in the fractions that eluted at both 30 and 32 min in panel A were determined by mass spectrometry and only one peptide with MH^+ of 1722.29 Da was found.

NMR studies on the binding of skeletal (*28*) and cardiac TnI (*31*) inhibitory peptides to TnC arrived at similar conclusions.

Conformation of TnC's Central Helix. We measured the distances from TnI residue 6 to TnC residues 12 (between the N- and A-helices), 41 (in the B-helix) and 89 (at the center of the central helix). In the ternary Tn complex, they are ~40, ~50, and ~33 Å, respectively (Table 2). These measured distances are compared with the corresponding distances calculated from two models: in the first (extended) model (*12*) TnI's N-terminal helix is bound to TnC's C-domain hydrophobic cleft as the crystal structure of TnC•TnI_{1-47} (*13*), but TnC's central helix is extended as in the crystal structures of free $2Ca^{2+}$•TnC (*3*). For this model in the $4Ca^{2+}$ state the conformation of TnC's N-domain is taken to be that in the crystal structure of $4Ca^{2+}$•TnC (*5*) (Figure 1B). The second (compact) model is identical to the crystal structure of TnC•TnI_{1-47} with the bent central helix (*13*). In this structure two Ca^{2+} are bound at TnC's C-domain sites and the N-domain hydrophobic cleft is closed. For this model in the $4Ca^{2+}$ state, we took the hypothetical structure

by these authors with the open TnC N-domain cleft, to which TnI segment 96−128 is bound (Figure 1C).

R(I6−C89) is similar for both models (∼25 and ∼31 Å for the compact and extended models, respectively), as might be expected, since the bending in the compact model occurs near TnC residue 89 (*13*). Although our measured distance (∼33 Å) is closer to the latter value, it cannot conclusively distinguish the two models. It does, however, further confirm that the conformation of TnI's N-terminal region and TnC's C-terminal region in intact Tn is similar to that in the crystal structure of TnC·TnI_{1-47}. For *R*(I6−C41) the compact model predicts a much shorter distance (by ∼25 Å) than the extended model, owing to the bend in TnC's central helix, bringing TnC's C-domain very close to its N-domain. Our measured values clearly conform more to the extended model. For *R*(I6−C12) the compact model likewise predicts a much shorter value (∼13 Å) than the extended model (∼31.5 Å), and our measured value (∼41 Å) is much closer to that of the extended model. However, our measured distance is significantly larger than the one calculated from the extended model (by ∼10 Å), raising the possibility that the true conformation of TnC in the Tn complex may not be exactly the same as that in the extended model. Overall, we believe that our results here conform better to the extended model than to the compact model. On the basis of their low-angle scattering results, structural models for TnC complexed with TnI have been proposed (*15, 16*). Although the two models differ substantially from each other, both are consistent with an extended conformation for TnC.

Both our photo-cross-linking and FRET results for the binary TnI·TnC complex are by and large similar to those for the Tn complex and therefore support the notion that TnC's central helix is extended in the binary complex as well. The exception is that in the $4Ca^{2+}$ state the $TnI6^{BP}$ photo-cross-linking site in TnC is Met43 in TnC's N-domain, and *R*(I6−C41) exhibits a multiplicity ranging from 32 to 47 Å. The lower value conforms well with the compact model value, while the higher value is similar to that predicted by the extended model. This is not likely to be due to dissociation of TnI's N-terminal region from TnC's C-domain cleft because *R*(I6−C89) under this condition (35 Å) is similar to those measured in the ternary complex and predicted by the extended model. We interpret these results as reflecting dynamic changes in TnC's conformation between a compact and an extended form. It is possible that in the absence of TnT, the central helix of TnC becomes flexible in the TnC·TnI binary complex, allowing TnI residue 6 to come into the proximity of TnC's B−C linker region. An increase in the flexibility of TnC's central helix under certain conditions is reported in other FRET (e.g., ref *32*) and NMR studies (e.g., ref *33*).

At first glance it may seem inconsistent that under the same conditions neither *R*(I6−C89) nor *R*(I6−C12) exhibits any multiplicity. In the former case, the distance between the two residues is relatively insensitive to bending of TnC's central helix (Figure 1, Table 2), so that no distance multiplicity can be expected. In the latter case, the distance between the two residues in the compact conformation (∼13 Å) is so short that the corresponding lifetime (0.02 ns) would be too short to be detectable in our instrument. Also, in the $2Mg^{2+}$ state $I6^{BP}$ photo-cross-links to TnC Ser133 in both the TnC·TnI and the Tn complex, but *R*(I6−C89) is significantly longer in the former complex. This apparently conflicting result may be another consequence of flexibility in the binary TnC·TnI complex. It is possible that under this condition the region containing TnC residue 89 is somewhat unfolded, giving rise to a larger distance of 41.5 Å. However, TnI residue 6 remains in the proximity of TnC Ser133 and undergoes benzophenone-mediated photo-cross-linking to it preferentially.

It seems clear, however, that such conformational dynamics do not occur in the ternary complex, indicating that the presence of TnT stabilizes the conformation of TnC and perhaps that of TnI as well. Previously we have shown that the distance between TnI residues 48 and 133 increases by 10 Å in going from the TnC·TnI to the Tn complex (*18*) and that TnT protects the inhibitory region of TnI from chymotryptic digestion (*34*). We also have evidence that TnI's inhibitory region interacts with TnC's central helix and that residues 48−89 of TnI, the region between TnI's N-terminal helix and the inhibitory region, interact with TnT (*12*). Taken together, it seems likely that TnT interacts with the N-terminal portion of TnI and the C-terminal portion of TnC and serves to stabilize the conformation of this region of the TnC·TnI complex. Our results here further emphasize that the conformations of TnC and TnI in the TnC·TnI complex are not the same as those in the ternary Tn complex.

In summary, our results show first that in the intact Tn complex TnC adopts an extended conformation. Second, TnI's N-terminal region is bound to TnC's C-domain cleft in both the activated and inhibited states of muscle and therefore plays mainly a structural role in Tn regulation. Finally, the presence of TnT in the ternary Tn complex may serve to stabilize TnC's central helix and maintain the latter's extended conformation.

ACKNOWLEDGMENT

We thank Dr. K. Langsetmo for assistance in the preparation of Figure 1. We thank Dr. Y. Maeda for sending us coordinates of the crystal structure of TnC·TnI_{1-47} prior to publication.

REFERENCES

1. Perry, S. V. (1999) *Mol. Cell. Biochem. 190*, 9−32.
2. Farah, C. S., and Reinach, F. C. (1995) *FASEB J. 9*, 755−767.
3. (a) Sundaralingam, M., Bergstrom, R., Strasburg, G., Rao, S. T., Greaser, M., and Wang, B. C. (1985) *Science 227*, 945−948. (b) Herzberg, O., and James, M. N. G. (1985) *Nature 313*, 653−659.
4. Herzberg, O., and James, M. N. G. (1988) *J. Mol. Biol. 203*, 761−779.
5. Houdusse, A., Love, M. L., Dominguez, R., Grabarek, Z., and Cohen, C. (1997) *Structure 5*, 1695−1711.
6. Soman, J., Tao, T., and Phillips, G. N. (1999) *Proteins: Struct., Funct., Genet. 37*, 510−511.
7. Herzberg, O., Moult, J., and James, M. N. G. (1986) *J. Biol. Chem. 261*, 2638−2644.
8. (a) Grabarek, Z., Tan, R.-Y., Wang, J., Tao, T., and Gergely, J. (1990) *Nature 345*, 132−135. (b) Fujimori, K., Sorenson, M., Herzberg, O., Moult, J., and Reinach, F. C. (1990) *Nature 345*, 182−184.
9. Tripet, B., Van Eyk, J. E., and Hodges, R. S. (1997) *J. Mol. Biol. 271*, 728−750.
10. (a) McKay, R. T., Tripet, B. P., Hodges, R. S., and Sykes, B. D. (1997) *J. Biol. Chem. 272*, 28494−28500. (b) McKay, R. T., Pearlstone, J. R., Corson, D. C., Gagne, S. M., Smillie, L.

B., and Sykes, B. D. (1998) *Biochemistry 37*, 12419−12430. (c) McKay, R. T., Tripet, B. P., Pearlstone, J. R., Smillie, L. B., and Sykes, B. D. (1999) *Biochemistry 38*, 5478−5489. (d) Li, M. X., Spyracopoulos, L., and Sykes, B. D. (1999) *Biochemistry 38*, 8289−8298.
11. Luo, Y., Leszyk, J., Qian, Y., Gergely, J., and Tao, T. (1999) *Biochemistry 38*, 6678−6688.
12. Luo, Y., Wu, J. L., Li, B., Langsetmo, K., Gergely, J., and Tao, T. (2000) *J. Mol. Biol. 296*, 899−910.
13. Vassylyev, D. G., Takeda, S., Wakatsuki, S., Maeda, K., and Maeda, Y. (1998) *Proc. Natl. Acad. Sci. U.S.A. 95*, 4847−4852.
14. (a) Farah, C. S., Miyamoto, C. A., Ramos, C. H. I., da Silva, A. C. R., Quaggio, R. B., Fujimori, K., Smillie, L. B., and Reinach, F. C. (1994) *J. Biol. Chem. 269*, 5230−5240. (b) Pearlstone, J. R., Sykes, B. D., and Smillie, L. B. (1997) *Biochemistry 36*, 7601−7606.
15. Olah, G. A., and Trewhella, J. (1994) *Biochemistry 33*, 12800−12806.
16. Stone, D. B., Timmins, P. A., Schneider, D. K., Krylova, I., Ramos, C. H. I., Reinach, F. C., and Mendelson, R. A. (1998) *J. Mol. Biol. 281*, 689−704.
17. Greaser, M. L., and Gergely, J. (1973) *J. Biol. Chem. 248*, 2125−2133.
18. Luo, Y., Wu, J.-L., Gergely, J., and Tao, T. (1997) *Biochemistry 36*, 11027−11035.
19. Wang, Z., Sarkar, S., Gergely, J., and Tao, T. (1990) *J. Biol. Chem. 265*, 4953−4957.
20. Tao, T., and Cho, J. (1979) *Biochemistry 18*, 2759−2765.
21. Small, E. W., and Isenberg, I. (1976) *Biopolymers 15*, 1093−1100.
22. Fairclough, R. H., and Cantor, C. R. (1978) *Methods Enzymol. 28*, 347−379.
23. Tao, T., Lamkin, M. L., and Lehrer, S. S. (1983) *Biochemistry 22*, 3059−3066.
24. Dalbey, R. E., Weiel, J., and Yount, R. G. (1983) *Biochemistry 22*, 4696−4706.
25. Tao, T., Qian, Y., Boldogh, I., and Gergely, J. (1995) *Biophys. J. 68*, A166.
26. Ngai, S. M., and Hodges, R. S. (1992) *J. Biol. Chem. 267*, 15715−15720.
27. (a) Dalgarno, D. C., Grand, R. J. A., Levine, B. A., Moir, A. J. G., Scott, G. M. M., and Perry, S. V. (1982) *FEBS Lett. 150*, 54−58. (b) Leszyk, J., Tao, T., Nuwaysir, L. M., and Gergely, J. (1998) *J. Muscle Res. Cell Motil. 19*, 479−490.
28. Mercier, P., Li, M. X., and Sykes, B. D. (2000) *Biochemistry 39*, 2902−2911.
29. (a) Meador, W. E., Means, A. R., and Quiocho, F. A. (1992) *Science 257*, 1251−1255. (b) Ikura, M., Clore, G. M., Gronenborn, A. M., Zhu, G., Klee, C. B., and Bax, A. (1992) *Science 256*, 632−638.
30. Xie, X., Harrison, D. H., Schlichting, I., Sweet, R. M., Kalabokis, V. N., Szent-Györgyi, A. G., and Cohen, C. (1994) *Nature 368*, 306−312.
31. Abbott, M. B., Dvoretsky, A., Gaponenko, V., and Rosevear, P. R. (2000) *FEBS Lett. 469*, 168−172.
32. (a) Wang, C.-L. A., Qian, Z., Tao, T., and Gergely, J. (1987) *J. Biol. Chem. 262*, 9636−9640. (b) Dong, W. J., Robinson, J. M., Xing, J., Umeda, P. K., and Cheung, H. C. (2000) *Protein Sci. 9*, 280−289.
33. Slupsky, C. M., and Sykes, B. D. (1995) *Biochemistry 34*, 15953−15964.
34. Tao, T., Gong, B. J., Grabarek, Z., and Gergely, J. (1999) *Biochim. Biophys. Acta 1450*, 423−433.

BI001259X